Journal of Diabetes Science and Technology
Volume 3, Issue 2, March 2009

SYMPOSIUM

Single Walled Carbon Nanotubes as Reporters for the Optical Detection of Glucose

Paul W. Barone, Ph.D. and Michael S. Strano, Ph.D.

Abstract

This article reviews current efforts to make glucose sensors based on the inherent optical properties of single walled carbon nanotubes. The advantages of single walled carbon nanotubes over traditional organic and nanoparticle fluorophores for *in vivo*-sensing applications are discussed. Two recent glucose sensors made by our group are described, with the first being an enzyme-based glucose sensor that couples a reaction mediator, which quenches nanotube fluorescence, on the surface of the nanotube with the reaction of the enzyme. The second sensor is based on competitive equilibrium binding between dextran-coated nanotubes and concanavalin A. The biocompatibility of a model sensor is examined using the chicken embryo chorioallantoic membrane as a tissue model. The advantages of measuring glucose concentration directly, like most optical sensors, versus measuring the flux in glucose concentration, like most electrochemical sensors, is discussed.

J Diabetes Sci Technol 2009;3(2):242-252

Introduction

For the 194 million people afflicted with diabetes worldwide,[1] the key issue is meeting blood glucose and glycated hemoglobin targets.[2–4] Meeting targets in blood glucose is largely dependent on sensor technology. A reliable and simple-to-use sensor allowing continuous monitoring would impact both patient behavior and glucose control. Next-generation sensor technology is focused on continuous, *in vivo* analyte detection.[5–7] Current glucose sensors that are Food and Drug Administration approved for use in humans are electrochemical in nature[8] and take the form of devices that work via a transdermal electrode that require frequent replacement every few days to models in development utilizing telemetry, which require some form of surgical implantation.[9] Sensors based on optical signal transmission instead can either be minimally invasive, implanted fluorescence-based devices or involve completely noninvasive spectroscopic detection techniques. Fluorescence-based devices often utilize fluorescence resonance energy transfer between fluorophores[10–13] or some type of competitive binding.[14,15] While noninvasive spectroscopic techniques would be the most desirable, they currently lack analyte specificity and dynamic range,[7] as detailed in reviews by Moschou *et al.*,[5] Wickramasinghe *et al.*,[6] and Wilson *et al.*[8]

Author Affiliation: Department of Chemical Engineering, Massachusetts Institute of Technology, Cambridge, Massachusetts

Abbreviations: (CAM) chorioallantoic membrane, (Con A) concanavalin A, (GOx) glucose oxidase, (MW) molecular weight, (nIR) near-infrared, (PEG) polyethylene glycol, (SWNT) single walled carbon nanotubes

Keywords: carbon nanotube, glucose sensor, fluorescence

Corresponding Author: Michael S. Strano, Ph.D., Department of Chemical Engineering, Massachusetts Institute of Technology, 77 Massachusetts Avenue, Cambridge, MA 02139; email address strano@mit.edu

Several photonics applications have been proposed for glucose sensing.[16,17] The required optical components for Raman-based schemes are extremely expensive.[16,17] A low-resolution fluorescence method would be more desirable because current instrumentation is already affordable and amenable to microfabrication technologies.[18] Additionally, a small fluorescence-based device could readily be implanted beneath the skin without requiring surgical procedures. **Figure 1** shows a schematic of a sensor based on nanotube fluorescence and the detection of nanotube fluorescence through the tissue of a rat.

Why Single Walled Carbon Nanotubes (SWNT)

Single walled carbon nanotubes are cylindrical tubes of graphite with diameters on the order of 1 nm and lengths up to several millimeters.[19,20] Their nanometer scale dimensions give rise to a host of interesting phenomena. Depending on how the graphite sheet is rolled, SWNT can be either semiconducting or metallic.[19,21] While SWNT have been used in a wide number of applications, from composites to transistors, they have received a large amount of interest in regards to sensing. Because of their one-dimensional nature and the fact that all atoms are surface atoms, SWNT are especially sensitive to surface adsorption events. Metallic SWNT have been used to enhance the performance of electrochemical sensors for the detection of a number of analytes ranging from DNA[22] to glucose.[23] Semiconducting SWNT have been used as field effect transistors for the detection of a wide variety of biomolecules; however, there is still some controversy about the ability of nanotubes to transduce specific biomolecular events. The discovery of SWNT near-infrared (nIR) fluorescence in 2002[24] opened a whole new avenue for sensing. Changing how the graphite sheet making up the nanotubes is rolled affects the optical properties. Smaller diameter nanotubes will have larger band gaps and thus higher energy absorption and fluorescence than those of tubes with larger diameters, with nanotube fluorescence ranging from 900 to 1600 nm.[24,25]

In the case of optical sensors, the maximum emitted signal detected from an implanted sensor is dependent on the fluorophore quantum yield[26–29] and the absorption of both excitation and emission light within the tissue.[30] Both of these factors together limit the fluorescent probe that can be used for this purpose. **Figure 2A** plots the absorbance of deoxygenated and oxygenated human whole blood, the dominant absorber in the human body, as a function of wavelength. Furthermore, photobleaching, which is a property of all organic[31] and nanoparticle

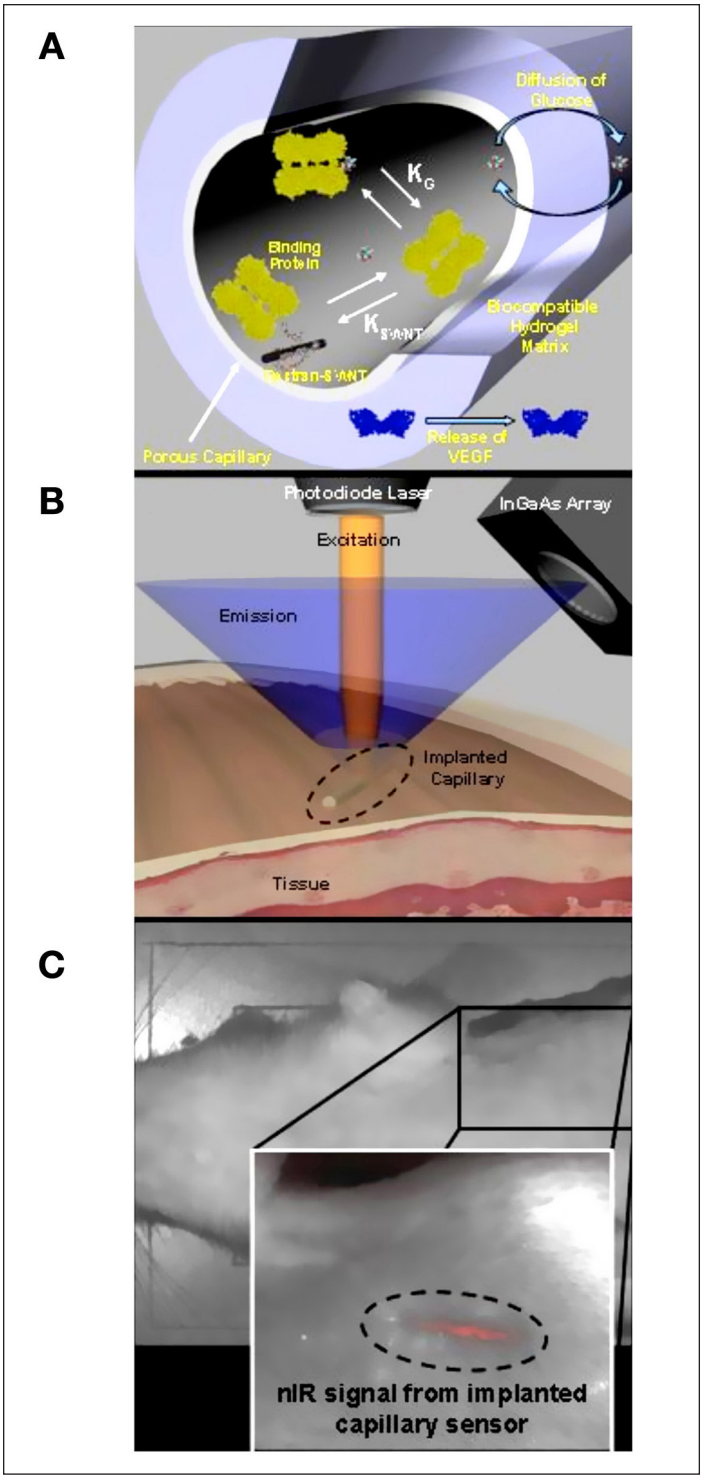

Figure 1. Implantable glucose sensor based on SWNT nIR fluorescence. **(A)** A porous dialysis capillary contains fluorescent glycosylated SWNT that shift their emission wavelength based on adsorption of a glucose-binding macromolecule. Free glucose diffuses into the capillary and replaces the bound entity, creating a reversible response. A porous, hydrogel allows slow release of angiogenic and anti-inflammatory factors to minimize fibrous encapsulation and biofouling. **(B)** The implanted device can be queried passively through the skin using near infrared light. **(C)** Image of SWNT-filled capillary embedded under rat skin acquired with the CRi Maestro *in vivo* imaging system with excitation from 649 to 690 nm, emission from 800 to 950 nm, a 5-second exposure, and 10 accumulations.

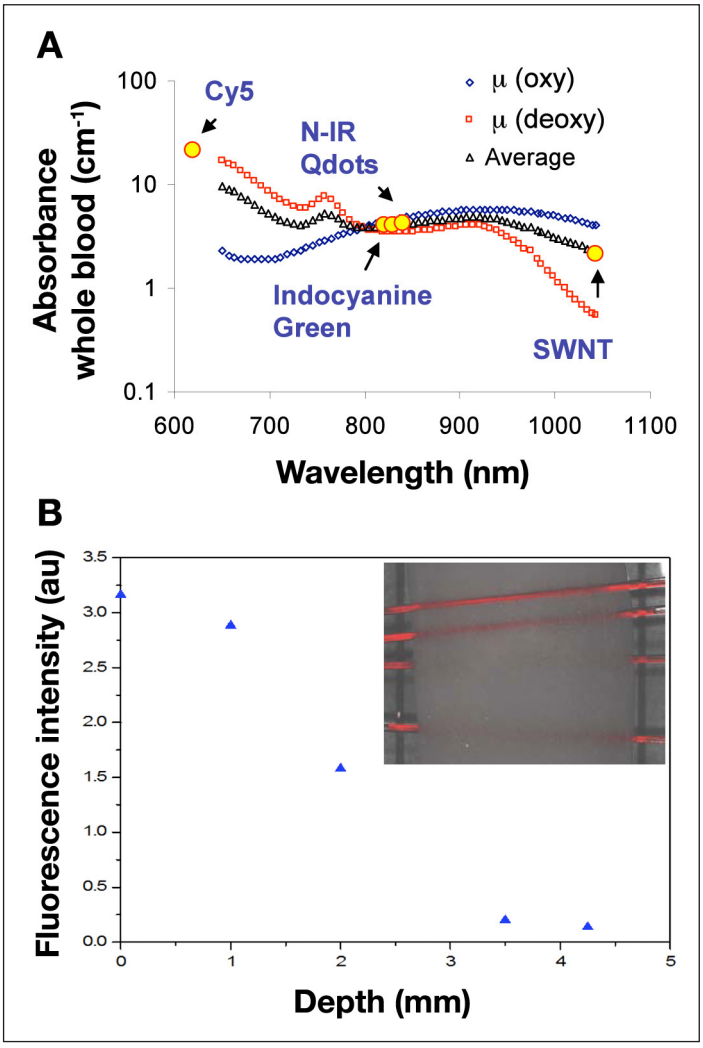

Figure 2. (A) Absorption coefficient of human whole blood (the dominant absorber for *in vivo* applications) for oxygenated, deoxygenated, and the average value. Potential fluorophores are compared. **(B)** Depth profile of a SWNT test sensor platform through chicken breast tissue. Measurement was made using the Maestro *in vivo* imaging system with excitation from 649 to 690 nm, emission from 800 to 950 nm, a 5-second exposure, and 10 accumulations. a.u., arbitrary unit. (Inset) nIR image of the SWNT-filled capillary proxy through chicken. The chicken breast is false colored in white, and the SWNT fluorescence is false colored in red.

fluorophores[32] investigated to date, except for carbon nanotubes,[33] will limit the viable sensor lifetime.

For an optical sensor-implanted distance, d, into tissue with absorption coefficient, μ, and fluorophore quantum yield, ϕ, a one-dimensional, absorption and fluorescence model can be used to estimate the signal intensity and lifetime of the device:

$$I_s = I_o \phi e^{-2\mu d - k\tau}, \quad (1)$$

where I_o is incident excitation intensity, I_s is fluorescent optical signal outside of the body, k is pseudo-first-order photobleaching rate constant, and τ is aggregate excitation exposure lifetime.

To maximize the signal detected from a sensor implanted a distance d into tissue, the fluorophore properties should be such that $\phi e^{-2\mu d}$ is maximized. **Table 1** shows this value calculated for common organic and nanoparticle fluorophores. It is obvious that visible fluorophores are significantly attenuated in a tissue sample and are not appropriate for implantable devices. Attenuation of visible fluorophore emission offsets the advantage of their higher quantum yield when compared with near-infrared dyes. Additionally, this analysis discounts interference from tissue autofluorescence, which disproportionately suppresses signals in the visible. **Figures 1C** and **2B** demonstrate the efficacy of measuring SWNT fluorescence through tissue. We should point out that the nanotube samples were not optimized for *in vivo* imaging.

The lifetime of any optical device is dependent on the stability of the fluorophore. For devices operating in a clinical setting, a maximum error of 20% can be tolerated for an *in vivo* glucose sensor before it is no longer viable.[9] For an optical sensor, the resulting limit for the working lifetime (τ) of the device is

$$\tau = -\frac{\ln(0.8)}{k}. \quad (2)$$

Table 2 uses photobleaching rate constants taken from literature data to estimate sensor lifetimes for some common visible and nanoparticle fluorophores. Organic fluorophores photobleach rapidly and are impractical for long-term applications. Even quantum dots, which possess bleaching rate constants several orders of magnitude lower than those of visible fluorophores, exhibit observable photobleaching.[32] Single walled carbon nanotubes are the only optical probe investigated to date that possesses no photobleaching threshold.[33,34]

Failure Mechanisms of Implantable Sensors

Klueh and co-workers[35,36] showed that placing cells that were genetically engineered to overexpress vascular endothelial cell growth factor induced significant neovascularization surrounding an implanted amperometric sensor for acetaminophen and later for glucose. The cells were placed in a hydrogel matrix, and the system was tested in an *ex ova* chicken embryo model. Results demonstrate that engineering neovascularization around the implant site can reduce undesired encapsulation effects dramatically.

Table 1.
Comparison of Commonly Utilized Visible and Near-Infrared Organic and Nanoparticle Fluorescent Probes Based on Quantum Yield (QY) and Absorbance in Human Whole Blood, (μ), the Dominant Absorbed in the Human Body

QY standards	QY (%)	Conditions for QY measurement	Excitation (nm)	μ (oxy) (cm^{-1})	μ (deoxy) (cm^{-1})	$\phi e^{-2\mu d}$ [a]
Cy5[26]	27	PBS[b]	620	2	60	3.20×10^{-28}
Fluorescein[28]	95	0.1 *M* NaOH, 22°C	496	150	120	5.23×10^{-118}
Rhodamine 6G[29]	95	Water	488	200	105	3.30×10^{-133}
Rhodamine B[29]	31	Water	514	110	190	1.60×10^{-131}
Indocyanine Green[27]	0.266	Water (0.15 g/liter)	820	0.96	0.77	4.72×10^{-4}
Indocyanine Green[27]	1.14	Blood (0.08 g/liter)	830	1.01	0.7788	1.91×10^{-3}
Type II NIR QD[32]	13	PBS	840	1.05	0.778	2.09×10^{-2}
SWNT[25]	0.1	PBS	1042	0.889	0.12	3.65×10^{-4}

[a] Based on a 1-cm-implanted sensor device, an average μ is utilized.
[b] Phosphate-buffered saline.

Table 2.
Comparison of Photobleaching Tendency of Common Organic and Nanoparticle Fluorophores[a]

Fluorescent probe	Photobleaching rate constant (h^{-1})	Fluence (mW/cm^2)	Nominal sensor lifetime
IR-Dye 78-CA[32]	250.92	600	3.2 s
Cy5[32]	20.52	600	39.1 s
Indocyanine Green[31]	0.0412	28	5.4 h
Type II NIR QD[32]	0.0827	600	2.7 h
SWNT[33]	0	1.0×10^6	α

[a] Estimated optical sensor device lifetime is calculated from Equation (2).

Norton and co-workers[37] have proposed several antifouling coatings to circumvent these common failure mechanisms. The hydrogels serve multiple functions, including an overall resistance to cell adhesion and as a matrix to deliver anti-inflammation and angiogenic agents. Several different configurations were examined, and it was found that delivery of these agents through hydrogel decomposition was superior to embedded microspheres as delivery vehicles. Hydrogels[38] themselves are excellent implant coatings due to biocompatibility and overall resistance to biofouling.[37,39]

While significant literature points to the clear advantage of this approach (combined hydrogel delivery of anti-inflammation and neovascularization factors),[35–37,39,40] it has not been conclusively demonstrated to work with an optical sensor device.

Concerns about Nanotube Toxicity

The toxicity of single walled carbon nanotubes is still in the early stages of exploration. While it has been shown that nanotubes implanted in the abdominal cavity of mice show a similar immunological response to asbestos, this toxicity was size dependent with a nanotube bundle length greater than 20 μm necessary for a response.[41] Several researchers, including our group,[42] have examined the cytotoxicity of SWNT in various eukaryotic cells. The majority of investigations have been concerned with drug or gene delivery where SWNT, suspended by a biomolecule, were tagged with a fluorophore for observation.[43–45] Two of these studies[43,44] used covalently functionalized SWNT, which exhibit a greatly reduced Raman and absorption cross section[46] and quenched photoluminescence.[24] One study[34] used the band gap fluorescence of surfactant-suspended SWNT to assess the toxicity of nanotubes in macrophages. The study showed nanotube fluorescence in cells only up to 24 hours after incubation, and the mechanism of intake was only applicable to cells that undergo phagocytosis. A larger study[42] has demonstrated no cytotoxicity at a high concentration (100 mg/ml) after a 3-month time period.[42] Additionally, nanotubes injected into rabbits demonstrated no toxic side effects over 24 hours[47] as did nanotubes injected into mice for a 3-month period.[48] There is even evidence of nanotube excretion once inside the body.[49]

Nanotube-Based Glucose Sensor

Enzyme-Based Optical Glucose Sensor

The central challenge in the fabrication of SWNT-based optical sensors is designing a sensor that maintains the nanotube optical properties while providing a selective analyte-binding site. Covalent functionalization necessarily disrupts the electronic structure of the nanotube, and thus its optical properties.[50] Therefore, only noncovalent methods may be used. The first example of glucose detection using SWNT fluorescence was demonstrated with a glucose oxidase (GOx)–SWNT optical sensor using a recently developed dialysis method to assemble functional proteins onto solution-suspended SWNT.[51] A target protein is combined with SWNT dispersed with a meta-stable surfactant and is dialyzed against surfactant-free buffer. Van der Waals forces alone can immobilize the protein monolayer, as demonstrated for glucose oxidase (**Figure 3**). **Figure 3A** shows nanotube fluorescence during the assembly process. The 10-meV shift in the emission maximum (**Figure 3A**, inset) confirms that the tightly packed surfactant phase has been replaced by an enzyme layer. Images show heights of 4.4 nm along the 1-nm-diameter nanotube consistent with an adsorbed dimer (**Figure 3B**).

Once the glucose oxidase is assembled, an electroactive species such as potassium ferricyanide, $K_3Fe(CN)_6$, can irreversibly adsorb at the surface of the nanotube and shift the Fermi level into the valence bands or quench the emission after photoexcitation.[51] This functionality can be partially reduced, as glucose oxidase catalyzes the reaction of β-D-glucose to the D-glucono-1,5-lactone with a H_2O_2 coproduct. The partial reduction of potassium ferricyanide at 37°C and pH 7.4 can reversibly couple the carbon nanotube fluorescence to the glucose concentration.[51] The solution can be loaded into a sealed dialysis capillary where glucose is free to diffuse across the capillary boundary while the nanotube-sensing complex is retained (**Figure 4**). This capillary is imaged easily in the nIR through a human epidermal tissue sample. The fluorescence of one nanotube is shown to respond to glucose after an 80-second transient, even in a

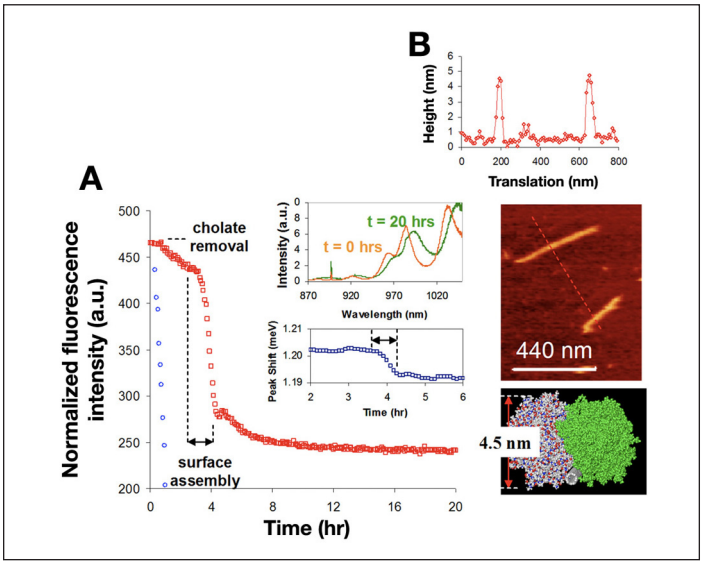

Figure 3. (A) Dialysis in the presence of glucose oxidase yields protein-stabilized nanotubes as monitored optically using transient emission. In the absence of enzyme (blue), the system aggregates rapidly. Assembly can be tracked using the 10-meV shift in wavelength (inset). a.u., arbitrary unit. **(B)** Atomic force microscope images of enzyme-suspended nanotubes on mica reveal average heights of 4.4 nm that correspond to a monolayer of dimers.

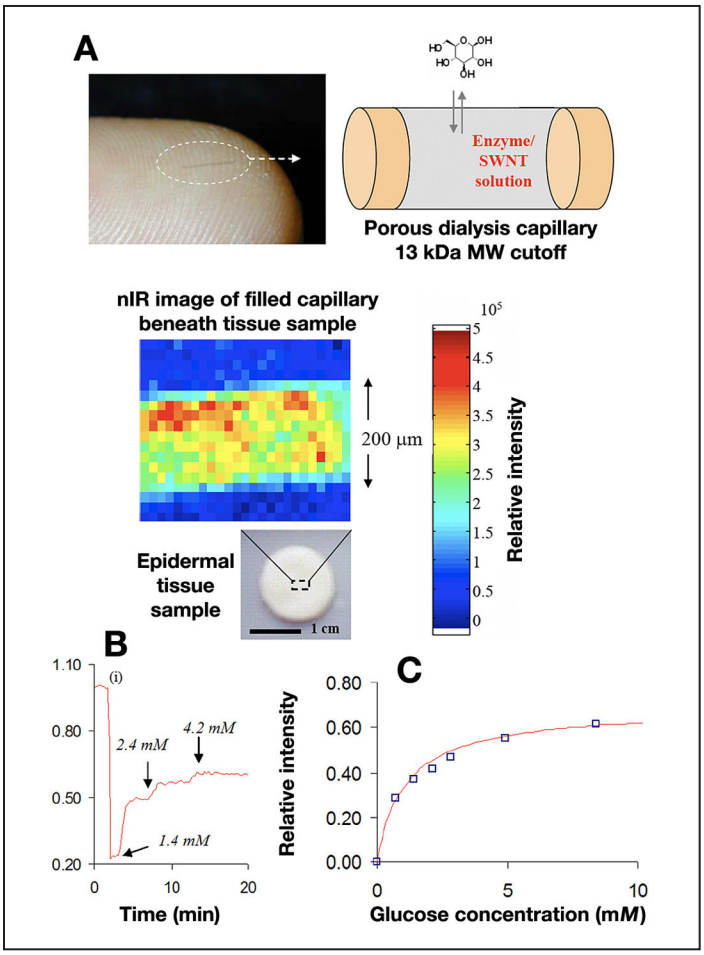

Figure 4. (A) A 200 μm × 1 cm, 13-kDa microdialysis capillary, shown to scale on a human finger, is loaded with the nanotube solution allowing glucose to diffuse through the membrane with containment of the sensing medium. Placing the capillary beneath a human epidermal tissue sample (above), we can clearly map the nanotube fluorescence from the capillary, seen in the two-dimensional profile. **(B)** After ferricyanide surface reaction at 37°C and pH buffered at 7.4 (i), the fluorescence response to the addition of 1.4, 2.4, and 4.2 m*M* glucose is scaled by the difference between minimum and maximum intensities. **(C)** The response function relates the normalized intensity to the local glucose concentration in the range of blood glucose detection with a type I absorption isotherm.

whole blood specimen maintained at 37°C and pH 7.4. The detection limit is approximately 2.2 molecules per nanometer of nanotube length.

Protein Affinity-Based Optical Glucose Sensor

The prototype described in **Figures 3** and **4** is based on GOx and is limited by cofactor regeneration. Additionally, the GOx–SWNT sensor operates in a flux-based manner, with the same disadvantages of flux-based sensors discussed later. A more robust scheme would be both reversible and not require regeneration. As such, the next generation in SWNT sensor design is focused on utilizing protein competitive binding to make a SWNT-based glucose affinity sensor. **Figure 5** shows the general sensor design. The nanotube is first coated in dextran, which is a glucose analogue. The addition of concanavalin A (Con A), a lectin with four glucose-binding sites, will induce protein-controlled aggregation and a SWNT fluorescence decrease, as the number of nanotubes free in solution is decreased. The introduction of glucose will cause the equilibrium to shift and dissolution of the aggregate in conjunction with fluorescence recovery.[52]

As nanotubes are inherently hydrophobic and dextran is a very hydrophilic polymer, it is first necessary to functionalize the dextran with hydrophobic phenoxy moieties. Increasing the weight percent phenoxy content from 0 to 8 wt% results in the increase of the number of nanotube in solution, where dextran alone is not capable of suspending nanotubes in solution. Again, a gentle dialysis method is used to assemble dextran on the nanotube surface.

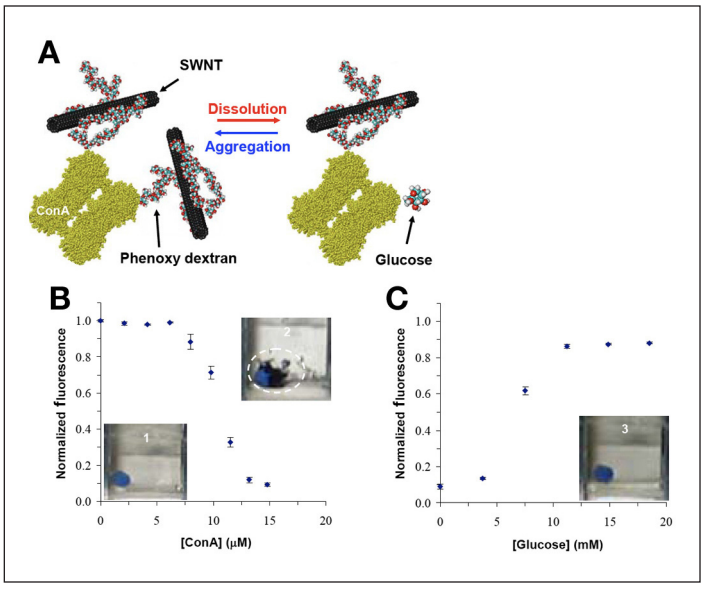

Figure 5. (A) Schematic of affinity glucose sensor operation. Dextran-coated nanotubes will aggregate in the presence of Con A, decreasing measured fluorescence. The addition of glucose results in aggregate dissolution and fluorescence recovery. **(B)** The addition of Con A to dextran-suspended nanotubes results in a 90% decrease in SWNT fluorescence and visible nanotube aggregation. **(C)** The subsequent addition of glucose causes nanotube aggregate dissolution and fluorescence recovery.

The addition of Con A to the phenoxy–dextran-stabilized nanotubes results in nanotube aggregation and a fluorescence decrease. A minimum amount of Con A is necessary before large enough nanotube aggregates are formed to cause a decrease in fluorescence. At a Con A concentration between 0 and 5.4 m*M*, the aggregate size is small enough to remain in solution and add to the total fluorescence signal, but at concentrations larger than 5.4 m*M* the aggregates attain a size such that they begin to settle out of solution and are no longer excited by the laser. Additions of glucose reverse this effect. This is the first demonstration of a reversible affinity sensor using single walled carbon nanotubes.[52] We note that the current sensor design is not sensitive to glucose over a wide enough range and would need to be designed to cover 2–30 m*M*.[9]

Effect of Sensor Architecture

Modeling Optical Sensor Dynamics

To compare the dynamics of optical and electrochemical glucose sensors, we consider the transient glucose response of a model, a well-controlled patient with basal insulin provided in response to three meals per day with t = 0 at 6 a.m.: a 40-gram breakfast at t = 60 minutes (7 a.m.); a 50-gram lunch at t = 360 minutes (12 p.m.); and a 100-gram dinner at t = 720 minutes (6 p.m.). The model of Lehmann and Deutsch[53] was used to calculate meal metabolism dynamics. **Figure 6A** compares blood glucose dynamics predicted by Sorensen,[54] with 80–349 mg/dl glucose, and Bergman and colleagues,[55] with concentration ranges of 80–172 mg/dl. The mass transport model of Schmidtke and colleagues[56] was used to calculate the resulting subcutaneous glucose dynamics based on the blood glucose response (**Figure 6B**) and resulted in a time lag of about 30 minutes between blood and glucose concentrations due to mass transfer resistance.

Biofouling Stability

The two major limitations to sensor operation *in vivo* are foreign body encapsulation[36,57–60] and membrane biofouling of the sensor surface.[39,61] Foreign body encapsulation, such as fibroblast encapsulation at the site of implantation, has been reviewed elsewhere,[58,59] and a number of possible solutions have been proposed.[35,36,39,40,61–66]

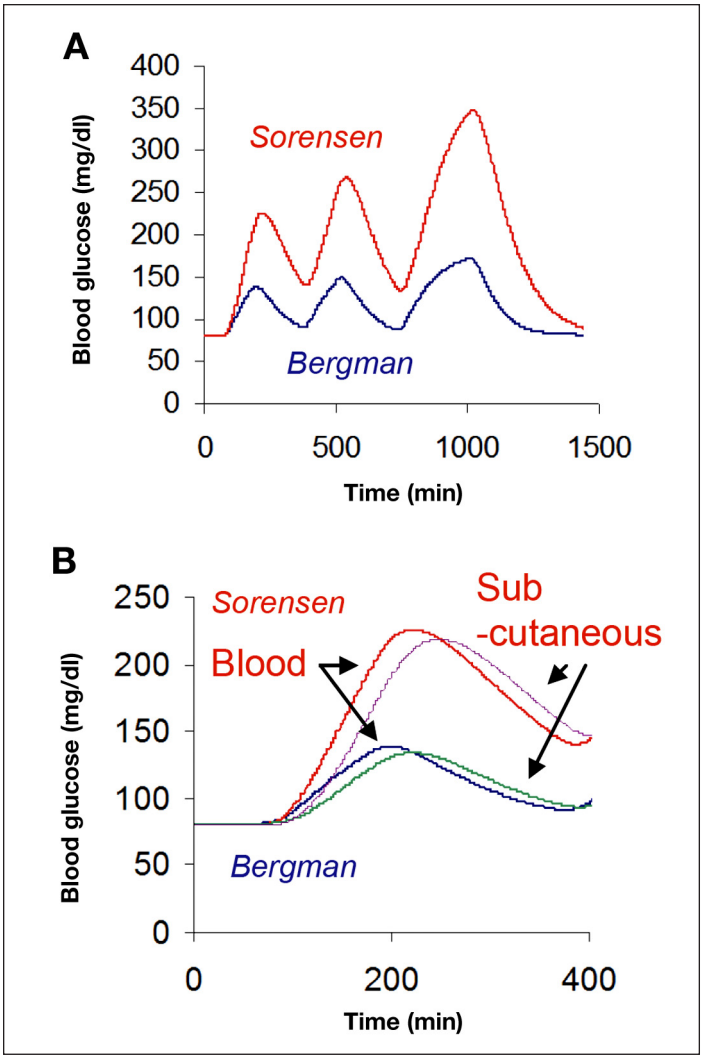

Figure 6. (A) Simulation of blood glucose levels of a healthy patient using the Sorensen (red) and Bergman (blue) models and a three-meal protocol described in the text. **(B)** Calculated subcutaneous glucose profiles using a mass transport model with a rate constant of 0.04 min^{-1} showing a 30-minute lag for both models

Biofouling of the sensor membrane, via either cell or protein adhesion, is the second problem with adherent bodies either blocking glucose transport or consuming glucose locally.[39,61] In doing so, the measured concentration is decreased relative to the value in the blood. As biofouling worsens over time, the difference between actual blood glucose, C_B, and measured glucose, C_s, increases until the sensor is no longer viable.

Sensor architecture can play a significant role in acerbating or ameliorating the effect of biofouling on the sensor. Biofouling at the sensor membrane necessarily limits the flux of glucose to the sensor as cellular adhesion becomes more pronounced. A review has been published elsewhere.[34] The simplest possible biofouling model is a first-order process that decreases the sensor membrane area, $A(t)$, from its initial value, A_o, with rate constant k_f:

$$A(t) = A_o e^{-k_f t} \quad (4)$$

Electrochemical sensors do not measure glucose directly but instead measure the flux of glucose through a limiting membrane. The signal, S, is proportional to the flux, J:

$$S \alpha J = \frac{A(t)D}{L}(C_B - C_S) \qquad \text{electrochemical sensor (5)}$$

Here, D is the membrane diffusivity of glucose [6.7×10^{-10} m^2/s for Alltech semipermeable membrane (Netherlands)[67]] and L is the membrane thickness. Fouling decreases the measured signal immediately and can be corrected only by frequent recalibration and eventual replacement.

In contrast, for an optical sensor that directly measures glucose concentration at the sensor, C_s, fouling only adds a mass transfer resistance with an ultimate delay in sensor response. However, this delay is not realized until the rate of glucose across the sensor membrane becomes commensurate with the rate of change of blood glucose:

$$S \alpha C_S$$

$$\frac{dC_S}{dt} = \frac{A(t)D}{LV}(C_B - C_S) \qquad \text{optical sensor (6)}$$

Figure 7A compares a model electrochemical sensor and an optical sensor subjected to a moderate biofouling rate constant of 5×10^{-5} min^{-1} and an initial sensor area of 2×10^{-6} cm^2. Biofouling distorts the signal measured by the electrochemical sensor immediately, with a loss of 20% of its accuracy after 3.7 days. However, a sensor that instead measures concentration directly is stable for more than 76 days after implantation, under identical conditions.

Sensor Biocompatibility and Fabrication

Evaluation of Dialysis Capillary Biocompatibility

Initial studies of capillary sensor biocompatibility have been performed using a chicken embryo chorioallantoic membrane (CAM) tissue model.[57] A shell-less culture was developed whereby chicken embryos were transplanted to plastic-covered cups after an initial 3-day incubation. The implant was then coated in egg white, to enhance incorporation, and placed onto the CAM after an additional 4 days of incubation. **Figure 8** shows the histological response after a 9-day incubation for an uncoated and polyethylene glycol (PEG) hydrogel-

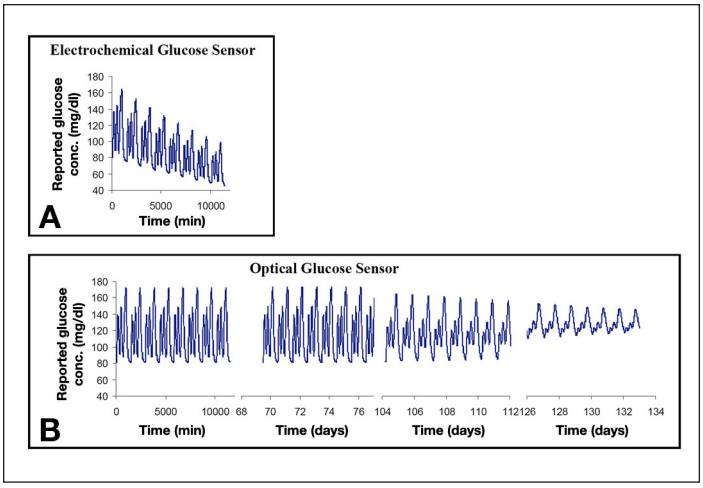

Figure 7. Effect of biofouling on the model responses of two types of glucose sensors. **(A)** An electrochemical sensor measures the flux of glucose to the electrode and exhibits signal distortion immediately as the effective membrane area is reduced. The sensor produces a 20% error after 3.7 days. **(B)** The same biofouling rate and initial area yield no diminution in an optical sensor response for more than 76 days. Constant parameter values were assumed for each sensor: $D = 6.7 \times 10^{-6}$ m^2/s, $L = 10^{-5}$, $A_0 = 2 \times 10^{-6}$ m^2, $V = 3.1 \times 10^{-10}$ m^3, $k_f = 5 \times 10^{-5}$ min^{-1}.

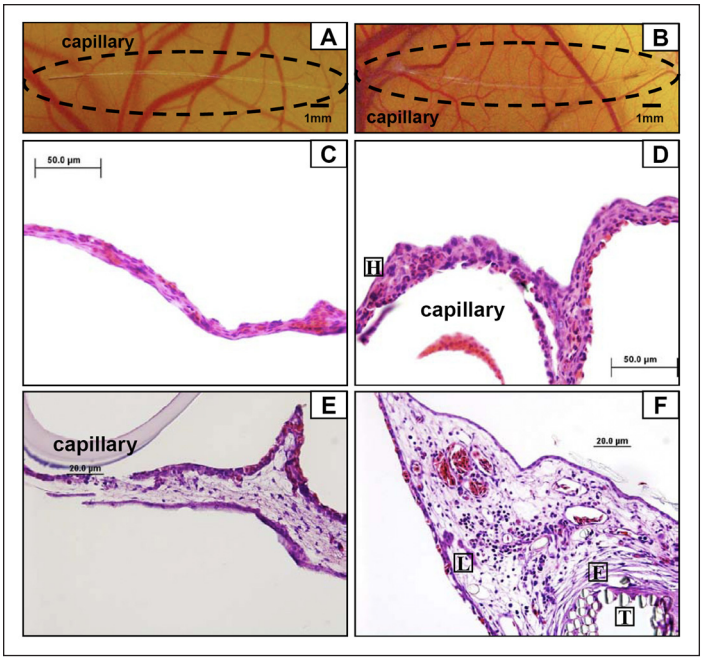

Figure 8. (A) A capillary placed on CAM for 2 hours. **(B)** A capillary placed on CAM for 9 days. **(C)** Hematoxylin and eosin (H&E) stain of normal CAM morphology. **(D)** H&E stain of capillary in CAM. A high density of heterophils and other acute inflammatory cells was observed around the capillary. **(E)** H&E stain of PEG-coated capillary in CAM. A very little inflammatory response was observed. **(F)** H&E stain of thread in CAM. Several layers of fibroblast encapsulation and severe inflammatory response were observed around the thread. H, heterophils; L, leukocytes (mostly macrophages and giant cells); F, fibroblast encapsulation induced by the thread; T, thread fibers within the tissue.

coated regenerated cellulose capillary and a polyester thread, used as a negative control. The hematoxylin and eosin-stained sections show that for the tissue surrounding the uncoated dialysis capillary, a high density of inflammatory cells, such as heterophils and giant mast cells, was present, whereas there was very little inflammatory response for the PEG-coated capillary. A severe inflammatory response and fibroblast encapsulation was observed around the thread. This shows that inflammation due to an implant in the CAM tissue model progresses from acute to chronic with associated fibrosis, similar to mammalian models, and can be used to prescreen the biocompatibility of implant materials.

Potential Interference from Protein Components in Whole Blood

False positive or negative readings from such a sensor may be caused by glucose-bearing proteins of low molecular weight (MW). **Table 3** outlines the principal components in plasma and blood with average molecular weight, carbohydrate content, and concentration.

The current sensor design utilizes a 13-kDa MW cutoff membrane separating the ambient tissue and fluid from the functionalized carbon nanotube. Excluding components above the cutoff and focusing on those with nonzero carbohydrate content leaves β-globulins as potentially interfering. Among this fraction, however, only β_2-microglobulin has a MW below the cutoff (11.7 kDa) of the sensor membrane. It is present in trace amounts and has no carbohydrate content. Thus, interference from such components in blood will be nonexistent. Testing in unseparated blood components is necessary, however, to demonstrate this fact.

Anticipated Device Fabrication Cost and Reproducibility

The final design of the 1-cm-implantable device utilizes 10 ng of carbon nanotube material. A conservative estimate of ~$1000/gram for this material and that of the hydrogel and dialysis coatings yield $0.17 per device. For excitation and collection optics, a number of vendors already offer hand-held, palm-based spectrofluorometers for under $2000 each. This provides an upper bound for the cost of data readout.

There has recently been significant progress in the ability to separate and prepare homogeneous carbon nanotube solutions, including methods from our group and others. Such methods will allow the production of a sensor based on SWNT fluorescence ratios. Different SWNT

Table 3:
Potential Interfering Components of Plasma and Blood Proteins

Protein	MW (Da)	Amount in Serum (mg/100 ml)	Percent Carbohydrate
Prealbumin	54,980	10 – 40	0
Retinol-binding protein	21,000	3 – 6	0
Albumin	66,500	0	0
Galactoglycoprotein	81,000	–	76
α-Globulins	26,000 – 725,000	Trace – 420	3 – 42
β-Globulins	11,730 – 440,000	Trace – 320	0 – 22
Low MW proteins	5,100 – 14,000	0.1 – 1.5	0
Complement components	71,000 – 400,000	1 – 120	0 – 9.4
Complement factors	24,000 – 540,000	2 – 35	0 – 10
Coagulation proteins	58,000 – 340,000	1 – 450	1.5 – 15
Immunoglobulins	23,000 – 950,000	Trace – 1800	0 – 10
β_2 Microglobulin	11,730	Trace	0
Lysozyme	14,000	0.5 – 1.5	
Basic Protein B_1	11,000	–	
Basic Protein B_2	8,800	<1	0
0.6 S γ_2-Globulin	5,100	<1	0
2 S γ_2-Globulin	14,000	0.1	0
Post γ-globulin	13,260	–	0

types fluoresce at distinct wavelengths. Combining SWNT with one emission wavelength, prepared to be nonanalyte responsive, with SWNT of another emission wavelength, prepared as the sensor, will give the sensor a method of internal calibration. Ratios between the peaks should yield accurate analyte concentrations regardless of changes in sensor depth or presence of local scatterers.

Conclusions

Single walled carbon nanotubes are an exciting class of materials that, as demonstrated, have a potential niche in *in vivo* sensor technology. A sensor based on nanotube fluorescence would avoid a number of complications that current sensing technology faces. Single walled carbon nanotube nIR fluorescence and photostability avoid *in vivo* transmission and sensor lifetime issues that most conventional fluorophores face. Additionally, a SWNT sensor that detects glucose directly should not be as affected by biofouling as a flux-based sensor. We have demonstrated two prototype SWNT-based glucose sensors: an enzyme-based sensor and an affinity sensor. The SWNT-based affinity sensor avoids inherent problems faced by flux-based sensors. Finally, initial biocompatibility testing regarding the sensing device has been carried out. These results form a promising beginning toward a nanotube-based *in vivo* continuous glucose monitoring device.

Acknowledgments:

The authors gratefully acknowledge a grant from the National Science Foundation (CTS-0330350), and PWB received funding from the School of Chemical Sciences at UIUC in the form of a Drickamer Graduate Fellowship.

References:

1. Diabetes atlas. 2nd ed. International Diabetes Federation; 2003.
2. The Diabetes Control and Complications Trial Research Group. The effect of intensive treatment of diabetes on the development and progression of long-term complications in insulin-dependent diabetes-mellitus. N Engl J Med. 1993;329(14):977-86.
3. Barnett AH. Treating to goal: challenges of current management. Eur J Endocrinol. 2004;151 Suppl 2:T3-7; discussion T29-30.
4. The absence of a glycemic threshold for the development of long-term complications: The perspective of the Diabetes Control and Complications Trial. Diabetes. 1996 Oct;45(10):1289-98.
5. Wickramasinghe Y, Yang Y, Spencer SA. Current problems and potential techniques in *in vivo* glucose monitoring. J Fluoresc. 2004;14(5):513-20.
6. Moschou EA, Sharma BV, Deo SK, Daunert S. Fluorescence glucose detection: advances toward the ideal *in vivo* biosensor. J Fluoresc. 2004;14(5):535-47.
7. Gough DA, Armour JC, Baker DA. Advances and prospects in glucose assay technology. Diabetologia. 1997;40 Suppl 2:S102-7.
8. Wilson GS, Gifford R. Biosensors for real-time *in vivo* measurements. Biosens Bioelectron. 2005;20(12):2388-403.
9. Heller A. Implanted electrochemical glucose sensors for the management of diabetes. Annu Rev Biomed Eng. 1999;1:153-75.
10. Pickup JC, Hussain F, Evans ND, Rolinski OJ, Birch DJ. Fluorescence-based glucose sensors. Biosens Bioelectron. 2005;20(12):2555-65.
11. McCartney LJ, Pickup JC, Rolinski OJ, Birch DJ. Near-infrared fluorescence lifetime assay for serum glucose based on allophycocyanin-labeled concanavalin A. Anal Biochem. 2001;292(2):216-21.
12. Cote GL. Noninvasive and minimally-invasive optical monitoring technologies. J Nutr. 2001;131(5):1596S-604S.
13. Rolinski OJ, Birch DJ, McCartney LJ, Pickup JC. A time-resolved near-infrared fluorescence assay for glucose: opportunities for trans-dermal sensing. J Photochem Photobiol B. 2000;54(1):26-34.
14. Ballerstadt R, Polak A, Beuhler A, Frye J. *In vitro* long-term performance study of a near-infrared fluorescence affinity sensor for glucose monitoring. Biosens Bioelectron. 2004;19(8):905-14.
15. Ballerstadt R, Schultz JS. A fluorescence affinity hollow fiber sensor for continuous transdermal glucose monitoring. Anal Chem. 2000;72(17):4185-92.

16. Berger AJ, Itzkan I, Feld MS. Feasibility of measuring blood glucose concentration by near-infrared Raman spectroscopy. Spectrochim Acta A Mol Biomol Spectrosc. 1997;53A(2):287-92.

17. Wang SY, Hasty CE, Watson PA, Wickstead JP, Stith RD, March WF. Analysis of metabolites in aqueous-solutions by using laser Raman spectroscopy. App Optics. 1993;32(6):925-9.

18. Kostov Y, Rao G. Low-cost optical instrumentation for biomedical measurements. Rev Sci Instruments. 2000;71:4361-74.

19. Dresselhaus MS, Dresselhaus G, Eklund PC. Science of fullerenes and carbon nanotubes. San Diego, CA: Academic Press; 1996.

20. Li QW, Zhang XF, DePaula RF, Zheng LX, Zhao YH, Stan L, Holesinger TG, Arendt PN, Peterson DE, Zhu YT. Sustained growth of ultralong carbon nanotube arrays for fiber spinning. Adv Mater. 2006;18(23):3160-3.

21. Saito R, Dresselhaus MS, Dresselhaus G. Physical properties of carbon nanotubes. London: Imperial College Press; 1998.

22. Wang SG, Wang R, Sellin PJ, Zhang Q. DNA biosensors based on self-assembled carbon nanotubes. Biochem Biophys Res Commun. 2004;325(4):1433-7.

23. Male KB, Hrapovic S, Liu YL, Wang DS, Luong JH. Electrochemical detection of carbohydrates using copper nanoparticles and carbon nanotubes. **Anal Chim Acta. 2004;516(1-2):35-41.**

24. O'Connell MJ, Bachilo SM, Huffman CB, Moore VC, Strano MS, Haroz EH, Rialon KL, Boul PJ, Noon WH, Kittrell C, Ma J, Hauge RH, Weisman RB, Smalley RE. **Band gap fluorescence** from individual single-walled carbon nanotubes. Science. 2002;297(5581):593-6.

25. Bachilo SM, Strano MS, Kittrell C, Hauge RH, Smalley RE, Weisman RB. Structure-assigned optical spectra of single-walled carbon nanotubes. Science. 2002;298(5602):2361-6.

26. Mujumdar RB, Ernst LA, Mujumdar SR, Lewis CJ, Waggoner AS. Cyanine dye labeling reagents: sulfoindocyanine succinimidyl esters. Bioconj Chem. 1993;4(2):105-11.

27. Benson R, Kues H. Fluorescence properties of indocyanine green as related to angiography. Phys Med Biol. 1978;23(1):159-63.

28. Lakowicz J. Principles of fluorescence spectroscopy. 2nd ed. New York: Kluwer Academic/Plenum; 1999.

29. Magde D, Rojas G, Seybold P. Solvent dependence of the fluorescence lifetimes of xanthene dyes. Photochem Photobiol. 1999;70(5):737.

30. Wray S, Cope M, Delpy DT, Wyatt JS, Reynolds EO. Characterization of the near infrared absorption spectra of cytochrome aa3 and haemoglobin for the non-invasive monitoring of cerebral oxygenation. Biochim Biophys Acta. 1988;933(1):184-92.

31. Saxena V, Sadoqi M, Shao J. Degradation kinetics of indocyanine green in aqueous solution. J Pharm Sci. 2003;92(10):2090-7.

32. Kim S, Lim YT, Soltesz EG, De Grand AM, Lee J, Nakayama A, Parker JA, Mihaljevic T, Laurence RG, Dor DM, Cohn LH, Bawendi MG, Frangioni JV. Near-infrared fluorescent type II quantum dots for sentinel lymph node mapping. Nat Biotechnol. 2004;22(1):93-7.

33. Graff RA, Swanson JP, Barone PW, Baik S, Heller DA, Strano SM. Achieving individual-nanotube dispersion at high loading in single-walled carbon nanotube composites. Adv Mater. 2005;17(8):980-4.

34. Cherukuri P, Bachilo SM, Litovsky SH, Weisman RB. Near-infrared fluorescence microscopy of single-walled carbon nanotubes in phagocytic cells. J Am Chem Soc. 2004;126(48):15638-9.

35. Klueh U, Dorsky DI, Kreutzer DL. Use of vascular endothelial cell growth factor gene transfer to enhance implantable sensor function *in vivo.* J Biomed Mater Res A. 2003;67(4):1072-86.

36. Klueh U, Dorsky DI, Kreutzer DL. Enhancement of implantable glucose sensor function *in vivo* using gene transfer-induced neovascularization. Biomaterials. 2005;26(10):1155-63.

37. Norton LW, Tegnell E, Toporek SS, Reichert WM. *In vitro* characterization of vascular endothelial growth factor and dexamethasone releasing hydrogels for implantable probe coatings. Biomaterials. 2005;26(16):3285-97.

38. Anseth KS, Metters AT, Bryant SJ, Martens PJ, Elisseeff JH, Bowman CN. *In situ* forming degradable networks and their application in tissue engineering and drug delivery. J Control Release. 2002;78(1-3):199-209.

39. Clark H, Barbari TA, Stump K, Rao G. Histologic evaluation of the inflammatory response around implanted hollow fiber membranes. J Biomed Mater Res. 2000;52(1):183-92.

40. Ward WK, Quinn MJ, Wood MD, Tiekotter KL, Pidikiti S, Gallagher JA. Vascularizing the tissue surrounding a model biosensor: how localized is the effect of a subcutaneous infusion of vascular endothelial growth factor (VEGF)? Biosens Bioelectron. 2003;19(3):155-63.

41. Poland CA, Duffin R, Kinloch I, Maynard A, Wallace WA, Seaton A, Stone V, Brown S, Macnee W, Donaldson K. Carbon nanotubes introduced into the abdominal cavity of mice show asbestos-like pathogenicity in a pilot study. Nat Nanotechnol. 2008;3(7):423-8.

42. Heller, D. A.; Baik, S.; Eurell, T. E.; Strano, M. S. Single-walled carbon nanotube spectroscopy in live cells: towards long-term labels and optical sensors. Adv Mater. 2005;17(23):2793-9.

43. Kam NW, Dai H. Carbon nanotubes as intracellular protein transporters: generality and biological functionality. J Am Chem Soc. 2005;127(16):6021-6.

44. Pantarotto D, Singh R, McCarthy D, Erhardt M, Briand JP, Prato M, Kostarelos K, Bianco A. Functionalized carbon nanotubes for plasmid DNA gene delivery. Angew Chem Int Ed Engl. 2004;43(39):5242-6.

45. Lu Q, Moore JM, Huang G, Mount AS, Rao AM, Larcom LL, Ke PC. RNA polymer translocation with single-walled carbon nanotubes. Nano Lett. 2004;4(12):2473-7.

46. Strano MS. Probing chiral selective reactions using a revised Kataura plot for the interpretation of single-walled carbon nanotube spectroscopy. J Am Chem Soc. 2003;125(51):16148-53.

47. Cherukuri P, Gannon CJ, Leeuw TK, Schmidt HK, Smalley RE, Curley SA, Weisman RB. Mammalian pharmacokinetics of carbon nanotubes using intrinsic near-infrared fluorescence. Proc Natl Acad Sci U S A. 2006;103(50):18882-6.

48. Schipper ML, Nakayama-Ratchford N, Davis CR, Kam NW, Chu P, Liu Z, Sun X, Dai H, Gambhir SS. A pilot toxicology study of single-walled carbon nanotubes in a small sample of mice. Nat Nanotechnol. 2008;3(4):216-21.

49. Singh R, Pantarotto D, Lacerda L, Pastorin G, Klumpp C, Prato M, Bianco A, Kostarelos K. Tissue biodistribution and blood clearance rates of intravenously administered carbon nanotube radiotracers. Proc Natl Acad Sci U S A. 2006;103(9):3357-62.

50. Strano MS, Dyke CA, Usrey ML, Barone PW, Allen MJ, Shan H, Kittrell C, Hauge RH, Tour JM, Smalley RE. Electronic structure control of single-walled carbon nanotube functionalization. Science. 2003;301(5639):1519-22.

51. Barone PW, Baik S, Heller DA, Strano MS. Near-infrared optical sensors based on single-walled carbon nanotubes. Nat Mater. 2005;4(1):86-92.

52. Barone PW, Strano MS. Reversible control of carbon nanotube aggregation for a glucose affinity sensor. Angew Chem Int Ed Engl. 2006;45(48):8138-41.

53. Lehmann E, Deutsch T. A physiological model of glucose-insulin interaction in type 1 diabetes mellitus. J Biomed Eng. 1992;14(3):235-42.

54. Sorensen JT. A physiologic model of glucose metabolism in man and its use to design and assess improved insulin therapies for diabetes [thesis]. Massachusetts Institute of Technology, Dept. of Chemical Engineering; 1985.

55. Bergman RN, Phillips LS, Cobelli C. Physiologic evaluation of factors controlling glucose tolerance in man. J Clin Invest. 1981;68(6):1456-67.

56. Schmidtke DW, Freeland AC, Heller A, Bonnecaze RT. Measurement and modeling of the transient difference between blood and subcutaneous glucose concentrations in the rat after injection of insulin. Proc Natl Acad Sci U S A. 1998;95(1):294-9.

57. Valdes TI, Klueh U, Kreutzer D, Moussy F. Ex ova chick chorioallantoic membrane as a novel *in vivo* model for testing biosensors. J Biomed Mater Res A. 2003;67(1):215-23.

58. Rebrin K, Fischer U, Hahn von Dorsche H, von Woetke T, Abel P, Brunstein E. Subcutaneous glucose monitoring by means of electrochemical sensors: fiction or reality? J Biomed Eng. 1992;14(1):33-40.

59. Abel PU, von Woedtke T. Biosensors for *in vivo* glucose measurement: can we cross the experimental stage. Biosens Bioelectron. 2002;17(11-12):1059-70.

60. Gerritsen M, Paquay YG, Jansen JA. Evaluation of the tissue reaction to a percutaneous access device using titanium fibre mesh anchorage in goats. J Mater Sci Mater Med. 1998;9(9):523-8.

61. Galeska I, Hickey T, Moussy F, Kreutzer D, Papadimitrakopoulos F. Characterization and biocompatibility studies of novel humic acids based films as membrane material for an implantable glucose sensor. Biomacromolecules. 2001 Winter;2(4):1249-55.

62. Levy AP, Levy NS, Loscalzo J, Calderone A, Takahashi N, Yeo KT, Koren G, Colucci WS, Goldberg MA. Regulation of vascular endothelial growth-factor in cardiac myocytes. Circ Res. 1995;76(5):758-66.

63. McColm J, Cunningham S. The development of a computer controlled system to simulate in rats, the rapid, frequent changes in oxygen experienced by preterm infants developing retinopathy of prematurity. J Med Eng Technol. 2000;24(2):45-52.

64. Pisano C, Aulicino C, Vesci L, Casu B, Naggi A, Torri G, Ribatti D, Belleri M, Rusnati M, Presta M. Undersulfated, low-molecular-weight glycol-split heparin as an antiangiogenic VEGF antagonist. Glycobiology. 2005;15(2):1C-6C.

65. Rusnati M, Urbinati C, Caputo A, Possati L, Lortat-Jacob H, Giacca M, Ribatti D, Presta M. Pentosan polysulfate as an inhibitor of extracellular HIV-1 Tat. J Biol Chem. 2001;276(25):22420-5.

66. Uhlmann S, Friedrichs U, Eichler W, Hoffmann S, Wiedemann P. Direct measurement of VEGF-induced nitric oxide production by choroidal endothelial cells. Microvasc Res. 2001;62(2):179-89.

67. Pijanowska DG, Sprenkels AJ, Olthuis W, Bergveld P. A flow-through amperometric sensor for micro-analytical systems. Sens Actuat. 2003;91(1-3):98-102.